# Recent progress on diaCEST MRI for tumor imaging
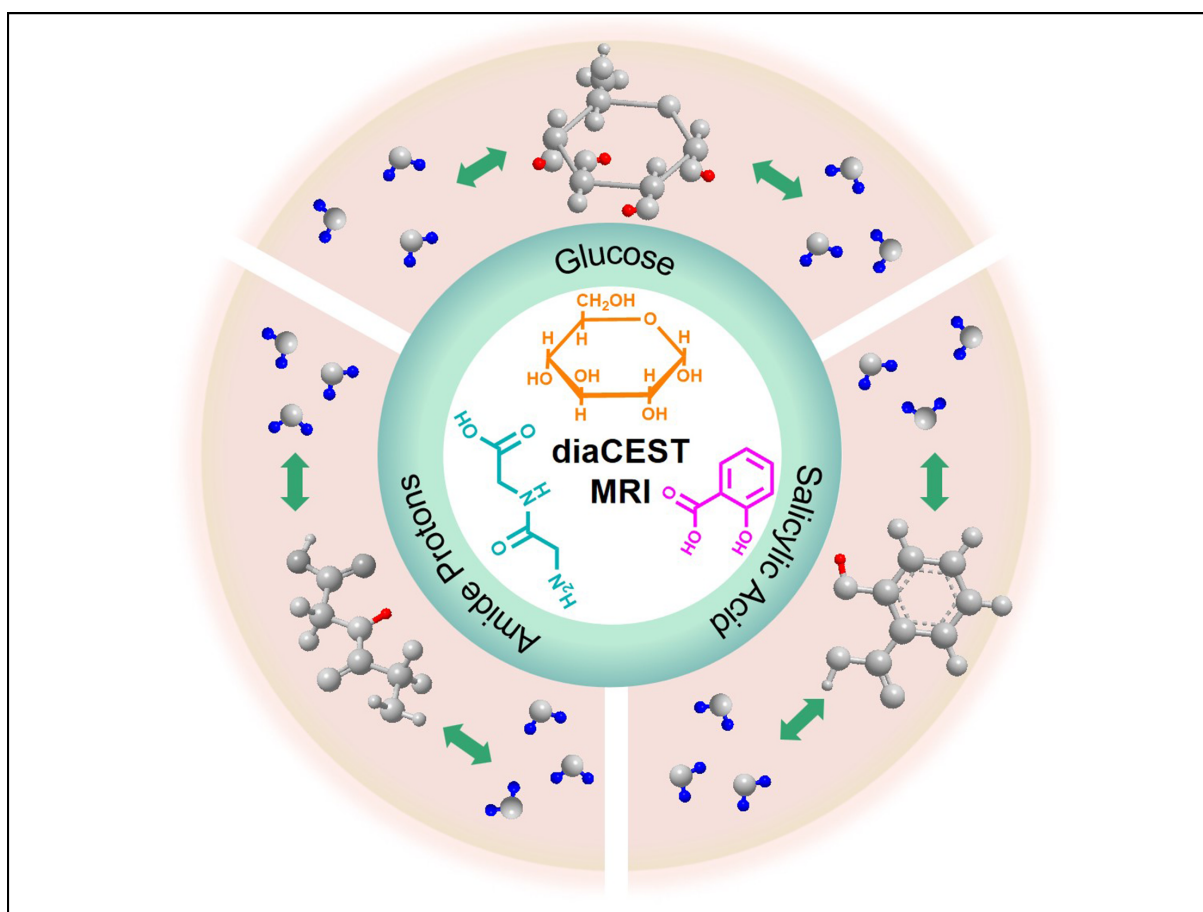
Qin Yu, Zian Yu, Lijiao Yang, and Yue Yuan ✉

*Department of Chemistry, University of Science and Technology of China, Hefei 230026, China*

✉Correspondence: Yue Yuan, E-mail: yueyuan@ustc.edu.cn

## Graphical abstract



*Three different diaCEST contrast agents and their chemical exchange saturation transfer process with bulk water protons.*

## Public summary

- We summarize several types of diaCEST MRI agents, including glucose, amide protons, salicylic acid and their analogs, which are promising for the diagnosis of tumors in CEST MRI.

- We present an in-depth discussion of the applications of these contrast agents in tumor imaging in recent years, such as colorectal tumors and brain tumors.

- We evaluate these three different types of contrast agents and point out their advantages and disadvantages in CEST MRI.

# Recent progress on diaCEST MRI for tumor imaging

Qin Yu, Zian Yu, Lijiao Yang, and Yue Yuan ✉

*Department of Chemistry, University of Science and Technology of China, Hefei 230026, China*

✉Correspondence: Yue Yuan, E-mail: yueyuan@ustc.edu.cn

**Abstract:** Chemical exchange saturation transfer (CEST) magnetic resonance imaging (MRI) is an advanced imaging method that probes the chemical exchange between bulk water protons and exchangeable solute protons. This chemical exchange decreases the MR signal of water and reveals the distribution and concentration of certain endogenous biomolecules or extrogenous contrast agents in organisms with high sensitivity and spatial resolution. The CEST signal depends not only on the concentration of the CEST contrast agent and external magnetic field but also on the surrounding environments of the contrast agent, such as pH and temperature, thus enabling CEST MRI to monitor pH, temperature, metabolic level, and enzyme activity in vivo. In this review, we discuss the principle of CEST MRI and mainly summarize the recent progress of diamagnetic CEST (diaCEST) contrast agents on tumor imaging, diagnosis, and therapy effect evaluation.

**Keywords:** chemical exchange saturation transfer; magnetic resonance imaging; diaCEST contrast agents; tumor imaging

**CLC number:** R445.2        **Document code:** A

## 1 Introduction

Chemical exchange saturation transfer magnetic resonance imaging (CEST MRI) is a relatively new MRI technology with rapid growth. Its underlying principle is applying an intended radio frequency (RF) pulse to stimulate the exchangeable protons in a specific agent or biomolecule and turn them into saturated states[1]. The saturation then will transfer to surrounding water protons by chemical exchange, resulting in a partial loss of bulk water signal. With a sufficient chemical exchange rate and saturation time, the saturated protons will constantly accumulate in bulk water. Therefore, the signal of water decreases significantly, which can be quantitatively detected by MR acquisition methods and indirectly reveals the distribution and concentration of the agent or biomolecule in vivo. Compared with conventional MRI technology, CEST MRI is capable of detecting diamagnetic molecules with high selectivity, sensitivity, and throughput. By virtue of various rationally designed bioinspired stimuli-responsive exogenous CEST contrast agents, such as pH, temperature, and metabolic level, CEST MRI has been reported to specifically detect many types of tissue lesions and tumors in vivo for medical diagnosis or treatment[2]. Moreover, the employment of diamagnetic contrast agents enables CEST MRI to track drug release and reveal important information such as the concentration and distribution of drugs in nanoparticle-based drug delivery systems (nano-DDS)[3]. Hence, diamagnetic CEST (diaCEST) has the potential to realize image-guided therapy and evaluate tumor aggressiveness, drug accumulation, and therapeutic response. In this review, we summarize the current status of diaCEST MRI for tumor imaging and introduce a series of diaCEST agents that have been reported for medical diagnosis and treatment in recent years, including glucose, salicylic acid and their analogs.

## 2 The underlying principle of CEST MRI

The underlying principle of CEST MRI is similar to that of magnetization transfer contrast (MTC), which can be simply explained by the two-pool model (Fig. 1)[4].

In this model, water protons are classified into two categories: exchangeable solute protons and bulk water protons. Exchangeable solute protons can be resonated by a specific frequency ($\Delta\omega$, $\omega$ is the saturation pulse frequency), which is different from that of bulk water protons. The large resonant frequency difference between exchangeable solute protons and water protons is preferred in CEST MRI to ensure that the exchangeable solute protons can be selectively saturated by using intended RF irradiation without influencing bulk water protons. The exchange between solute protons and bulk water protons will increase the number of saturated protons in the bulk water pool and slightly reduce the MR signal of bulk water protons. The unsaturated protons that transfer from the bulk water pool to the exchangeable solute pool can also be saturated by the intended RF irradiation. When the solute protons have sufficient exchange rates ($k_{sw}$) and saturation times
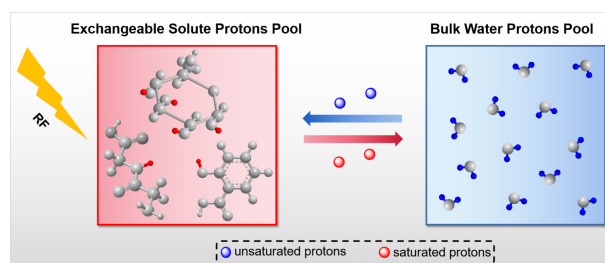
**Fig. 1.** The underlying principle of CEST MRI via a two-pool model.

($t_{sat}$), the saturated protons will continually be produced and ceaselessly transfer into the bulk water pool, resulting in an obvious drop in the bulk water signal. The signal loss of bulk water protons can be quantitatively detected after MRI data processing and indirectly reveal the concentration and distribution of the agents or biomolecules that exchange protons with bulk water (Fig. 2a).

The resonance frequency of bulk water protons is assigned to 0 ppm in CEST MRI, and the MR signal of water saturation ($S_{sat}$) was collected as a function of saturation frequency and normalized by the signal without saturation ($S_0$), which yields the so-called Z-spectrum, as shown in Fig. 2b. The frequency offset of the CEST peak ($\Delta\omega$) in the Z-spectrum is determined by the chemical shift between exchangeable solute protons and bulk water protons and thus is able to identify the type of solute. Since the water direct saturation is symmetric at approximately 0 ppm, the magnetization transfer ratio (MTR) asymmetric analysis of the Z-spectrum can efficiently eliminate the influence of direct saturation.

The definition of MTR is as follows:

$$\mathrm{MTR} = 1 - \frac{S_{sat}}{S_0}. \tag{1}$$

The definition of MTR asymmetric analysis is as follows:

$$\mathrm{MTR_{asym}} = \mathrm{MTR}(\Delta\omega) - \mathrm{MTR}(-\Delta\omega) = \frac{S_{sat}(\Delta\omega) - S_{sat}(-\Delta\omega)}{S_0}. \tag{2}$$

According to these formulas, the asymmetric analysis spectrum is shown in Fig. 2c.

Compared with conventional MRI methods, CEST MRI has several benefits. Different exchangeable solutes may resonate at different frequencies[5] (Fig. 3); thus, frequency-specific switchable contrast could be realized to provide information on multiple solutes independently in a single CEST image[6], which provides an excellent noninvasive strategy for studying the interlink of two or more biomolecules in a biological event. The employment of diamagnetic contrast agents is capable of tracking tumor metabolism[7], drug
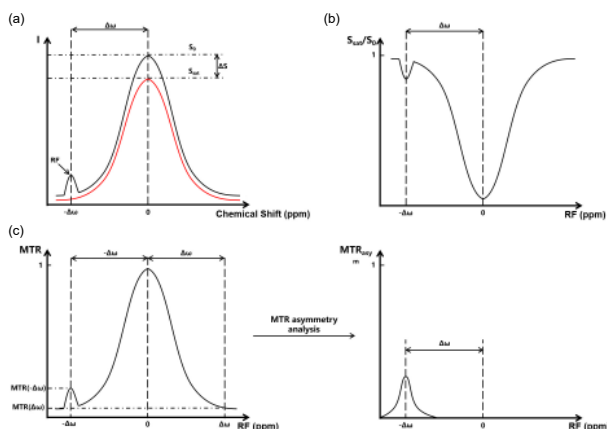


**Fig. 2.** The signal analysis and related spectrum. (a) The exchange of exchangeable solute protons and bulk water protons leads to a decrease in bulk water signals. Black line: signal intensity of water before RF irradiation; red line: signal intensity of water after RF irradiation. (b) Z-spectrum or CEST spectrum. (c) MTR asymmetry analysis.
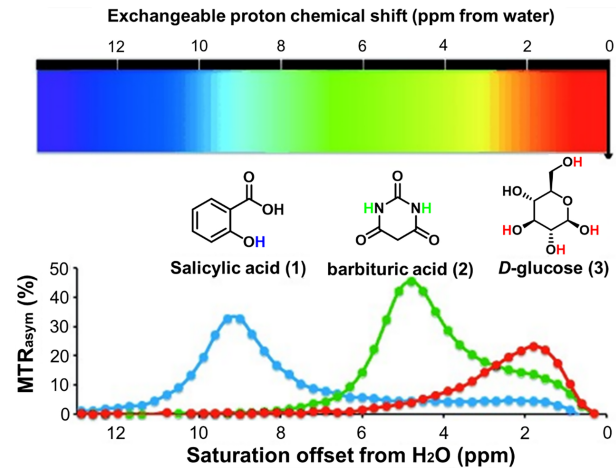


**Fig. 3.** Three different diaCEST contrast agents and their $\mathrm{MTR_{asym}}$ signals: Salicylic acid (1), barbituric acid (2), and D-glucose (3). Reprinted with permission from Ref. [8]. Copyright 2013, Springer Nature Limited.

biodistribution[3], cell transplantation[8], and other dynamic biological processes in vivo.

In addition, the type of exchangeable protons and environmental factors such as pH[8], temperature[9], enzyme activity[10] and metabolic level[11] will also affect CEST signals, which provides new ideas for CEST contrast agent design and greatly broadens the clinical application of CEST MRI technology. In more detail, both pH and temperature can accurately influence $k_{sw}$, which is sensitive to the Z-spectrum. The following formula reflects the relationship between $k_{sw}$ and pH, and the ability of CEST MRI to reflect different pH values makes it suitable for detecting renal injury, mapping the pH of tumors, and monitoring the viability of transplanted therapeutic cells[12].

$$k_{sw} = k_A 10^{-pH} + k_B 10^{[pH-pK_w]} + k_w,$$

where $k_A$ is the acid-specific exchange rate, $k_B$ is the base-specific exchange rate, $k_w$ is the proton exchange rate between water and exchangeable protons, and $pK_w$ is the water dissociation constant.

In addition, enzyme activity can alter CEST MRI signals through the reaction of the enzyme with diaCEST agents in vivo, leading to changes in the structures and functional groups of the agents. For instance, enzymes can initiate the self-assembly process of agents and enhance the signal intensity, thereby switching on the CEST MRI signal of the agents following the reaction[10].

# 3   CEST MRI contrast agents

Contrast agents are required in clinical MRI to improve the sensitivity and selectivity in the areas of interest. For CEST MRI, contrast agents are categorized into two types: paramagnetic CEST (paraCEST) contrast agents and diamagnetic CEST (diaCEST) contrast agents. Similar to traditional $T_1$ MRI contrast agents, paraCEST agents are chelates of lanthanide ions that induce larger chemical shifts of exchangeable protons in coordinated water or chelate structures, which can be shifted tens or even hundreds of ppm away from the solvent water peak, depending on the pseudo-contact shift (PCS) generated by paramagnetic metal ions

(Fig. 4)[6, 13]. A large value of $\Delta\omega$ for paraCEST contrast agents permits faster exchange conditions than diaCEST agents; however, the potential toxicity of paraCEST agents is an important factor we need to consider, especially that a relatively high dosage of contrast agent is required for CEST imaging.

Many endogenous substances can be applied as diaCEST contrast agents, including proteins[14], enzymes[15], and biomolecules containing amino and hydroxyl groups (e.g., glutamate[16], glucose[17], glycogen[18], and glycosaminoglycans[19]), and their labile protons can exchange with bulk water protons and produce CEST signals. These endogenous substances are abundant in vivo and have excellent biocompatibility, making them have considerable potentials to be widely employed in medical diagnosis. In addition, many drugs and nanocarriers, such as gemcitabine[20], citicoline[21], olsalazine (Olsa)[22], polyaminoamine (PAMAM)[23], and poly-L-lysine (PLL)[24], have abundant exchangeable protons, making them capable of producing CEST signals.

It is difficult for paraCEST contrast agents to achieve clinical translation owing to the complex synthesis process of paraCEST agents and the biotoxicity of lanthanide metal ions. Hence, diaCEST contrast agents are rapidly becoming a key point for CEST MRI technology[3]. Li et al.[25] reported a series of diaCEST contrast agents that possess deshielded labile protons, including salicylic acid and its analogs. Their structures are as follows (Fig. 5). The natural frequency difference between the diaCEST contrast agent and water is not too large, such as $\Delta\omega_{-OH} = 1$ ppm and $\Delta\omega_{-NH} = 3$ ppm; thus, their CEST signals are sensitive to $B_0$ of the MRI equipment, and slight fluctuations in $B_0$ may greatly influence the result of the MTR asymmetry analysis. Moreover, the resonance frequencies of the diaCEST contrast agent exchangeable protons are mostly distributed in a small interval around that of water protons, which may result in a serious background signal that cannot be neglected. To solve these problems, diaCEST agents with large natural frequency differences from water protons have attracted the attention of MRI researchers.

# 4   The application of diaCEST MRI in tumors

The employment of CEST MRI has generated significant interest in the domain of molecular imaging and quantitative biomarker analysis. This modality offers researchers valuable information such as the differentiation and grading of tumors,

as well as the pH value of tissues within the areas detected. Although diaCEST MRI has found extensive application in neuro-oncology research, its development in body oncology remains sluggish and requires further advancement[26]. At present, there are three major types of diaCEST agents utilized for tumor imaging: glucose and its analogs, amide protons, and salicylic acid (SA) and its analogs.

## 4.1   Glucose and its analogs

There are many hydroxyl groups in glucose and its analogs that can provide exchangeable protons for CEST MRI. To date, glucose and its analogs have been employed many times as excellent diaCEST contrast agents to reveal the distribution of tumor cells in vivo. One of the characteristic changes in the metabolic program of tumor cells is the increase in glucose uptake and lactate fermentation[27]. Even though glucose will be rapidly absorbed and translated into lactic acid by tumor cells, increased exogenous glucose uptake is a hallmark of solid tumors. Moreover, the acidic tumor microenvironment provides favorable conditions for CEST detection of glucose because it will slow down the rapid exchange of OH protons to increase the detection sensitivity[17]. All these factors enable CEST MRI based on glucose and its analogs to be a reliable imaging and diagnosis method for tumors.

Based on this, a natural biodegradable CEST MRI contrast agent, D-glucose, was employed by Chan et al.[17] for the detection of human breast cancer cells MDA-MB-231 and MCF-7 in mice. Obvious CEST signals from glucose (glucoCEST) were observed in both the MDA-MB-231 tumors and MCF-7 tumors, but the glucoCEST contrast of MDA-MB-231 tumors was significantly lower than that of MCF-7. The difference between the CEST signals from MDA-MB-231 tumors and MCF-7 tumors provides a new route to understand the microenvironment information of different tumor tissues (Fig. 6a–c), which cannot be identified by contradiitional Gd-enhanced MRI.

In 2013, Walker-Samuel et al.[28] used this glucoCEST technology to detect glucose uptake and metabolism in tumors, which could develop a simple, noninvasive, and cost-effective method for diagnosing disease and imaging therapy effects and provide an ideal substitution for the [18F]-fluorodeoxyglucose ([18F]FDG) positron emission tomography (FDG-PET) used in the clinic. GlucoCEST can sensitively reflect glucose uptake and accumulation conditions in
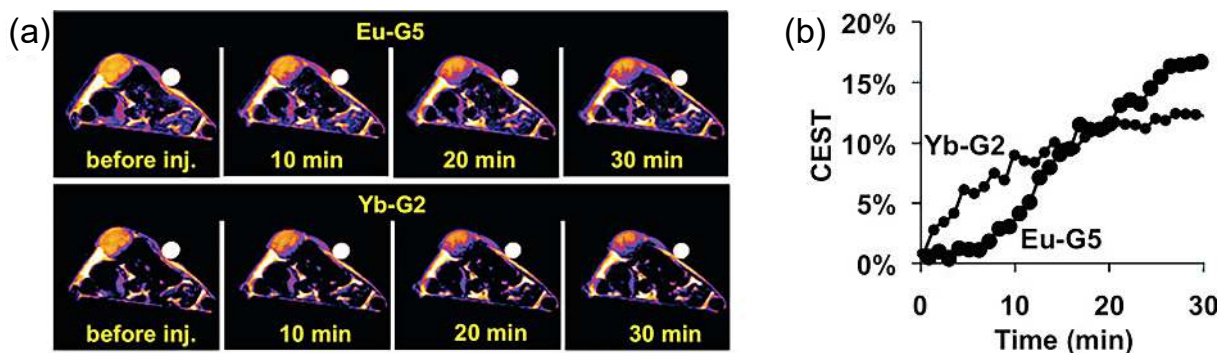


**Fig. 4.** Analysis of mouse tumors by paraCEST agents. (a) CEST serial MRI of tumor-bearing mice after injection of two different paraCEST agents and (b) quantitative CEST MRI signals of tumors at different time points. Reprinted with permission from Ref. [13]. Copyright 2009, American Chemical Society.
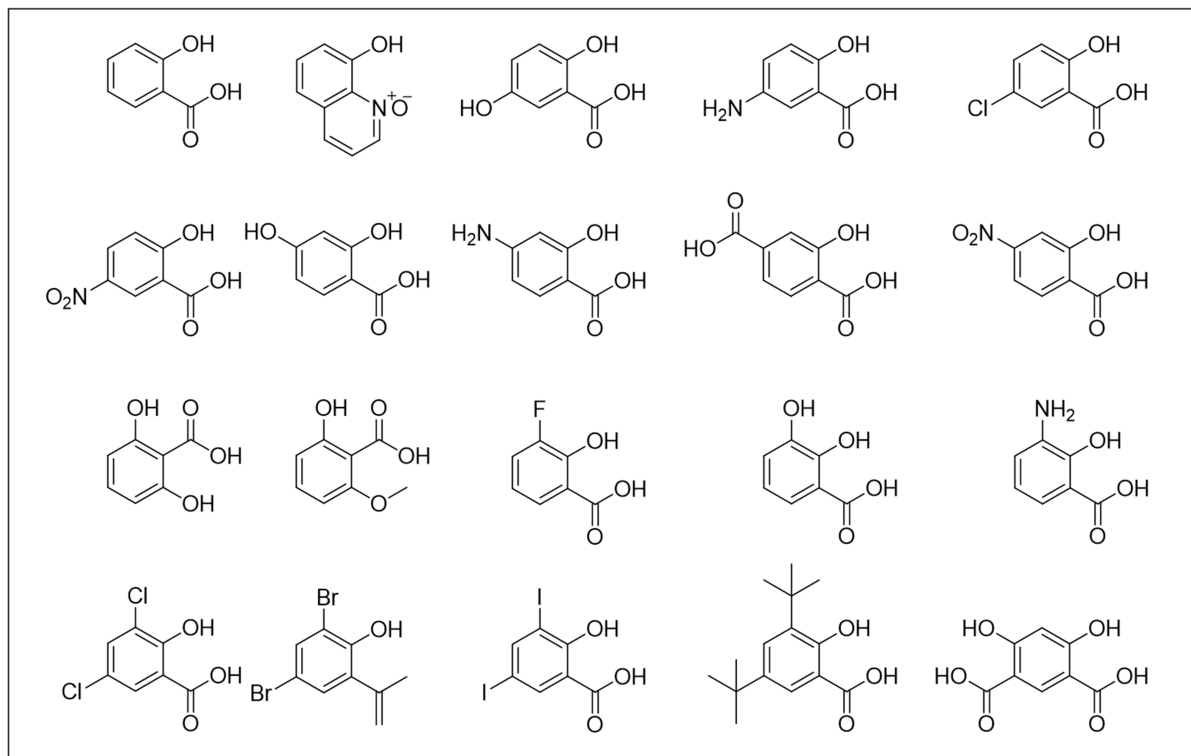
**Fig. 5.** Main structures of salicylic acid-based diaCEST contrast agents. Reproduced with permission from Ref. [25]. Copyright 2016, Wiley-VCH Verlag GmbH & Co. KGaA, Weinheim.

colorectal tumor mouse models and can identify tumor types (LS174T and SW1222) with different metabolic characteristics and pathophysiologies. They compared the imaging results of glucoCEST with the widely applied [18F]FDG and found that there is a strong consistency between these two contrast agents. Moreover, glucoCEST is not radioactive, which gives it more biosecurity than [18F]FDG and has excellent development prospects (Fig. 6d).

Considering that D-glucose is rapidly metabolized through glycolysis in tumors, its CEST signal may not be stable in vivo. Some glucose analogs, such as glucosamine, N-acetyl glucosamine[29], 2-deoxy-D-glucose[30], and dextran[31], that cannot be metabolized by cancer cells after uptake were developed as novel disCEST contrat agents. In 2019, Sehgal et al.[32] reported a new disCEST contrat agent, 3-O-methyl glucose (3-OMG). Their work demonstrated that 3-OMG can be used as a novel contrast agent for U87 brain tumor CEST imaging, and its CEST contrast is approximately 2-fold higher than that of D-glucose, benefitting from its nonmetabolizable feature, then it cannot be metabolized to lactate to quickly reduce the CEST signal. In contrast to D-glucose, the CEST signal of 3-OMG in tumor tissues was largely located in the intracellular space. Moreover, 3-OMG does not cause the accumulation of lactic acid in tumor tissues, which is more biocompatible than D-glucose (Fig. 6e, f). Based on this research, Anemone and coworkers[33] studied the difference in CEST signals between D-glucose and 3-OMG in a murine melanoma tumor model using CEST MRI. The results showed that both glucose and 3-OMG required a high magnetic field strength (7 T) to give better image qualities due to their small chemical shifts (0.8 ppm for glucose and 1.2 ppm

for 3-OMG). The major difference between them is the pH responsivity; 3-OMG exhibits higher glucoCEST signal intensity in a neutral environment than in an acidic environment, while glucose is completely opposite. After the intravenous injection of 3-OMG and D-glucose, the 3-OMG CEST contrast remained stable from 0 min to 30 min in the tumor region, but the glucoCEST signal showed a gradual increase as a result of the reduced pH value of the extracellular space by the release of lactic acid[34−36].

In the work of Nasrallah et al.[30], 2-deoxy-D-glucose (2-DG) and 2DG-6-phosphate (2DG6P) were applied to detect the uptake and metabolism of glucose via CEST MRI technology. They assessed the CEST MRI image of the rat brain with glucose, 2-DG, and 2DG6P and expounded the reasons for the different glucoCEST signal changes caused by them. 2-DG is a kind of glucose analog that can enter cells through the same transporters as D-glucose. It can be phosphorylated into 2DG6P by hexokinase, and then the formed 2DG6P will be deposited in the brain cells for several hours[37]. GlucoCEST signaling processes rapidly decay in the body after the injection of D-glucose because of rapid insulin secretion, cell metabolism and low sensitivity. However, 2-DG and 2DG6P were not affected by these factors. Since both of them will accumulate in brain cells, the changes in their glucoseCEST signals can directly reflect glucose assimilation, hexokinase activity, and other physiological parameters, such as pH and temperature, which can be applied in the clinical diagnosis and prognosis evaluation of cancer and inflammation.

Xylose (wood sugar), a kind of pentose sugar, is difficult for monogastric animal cells to metabolize[38]. In addition, xylose can cross the blood–brain barrier, which means that it can
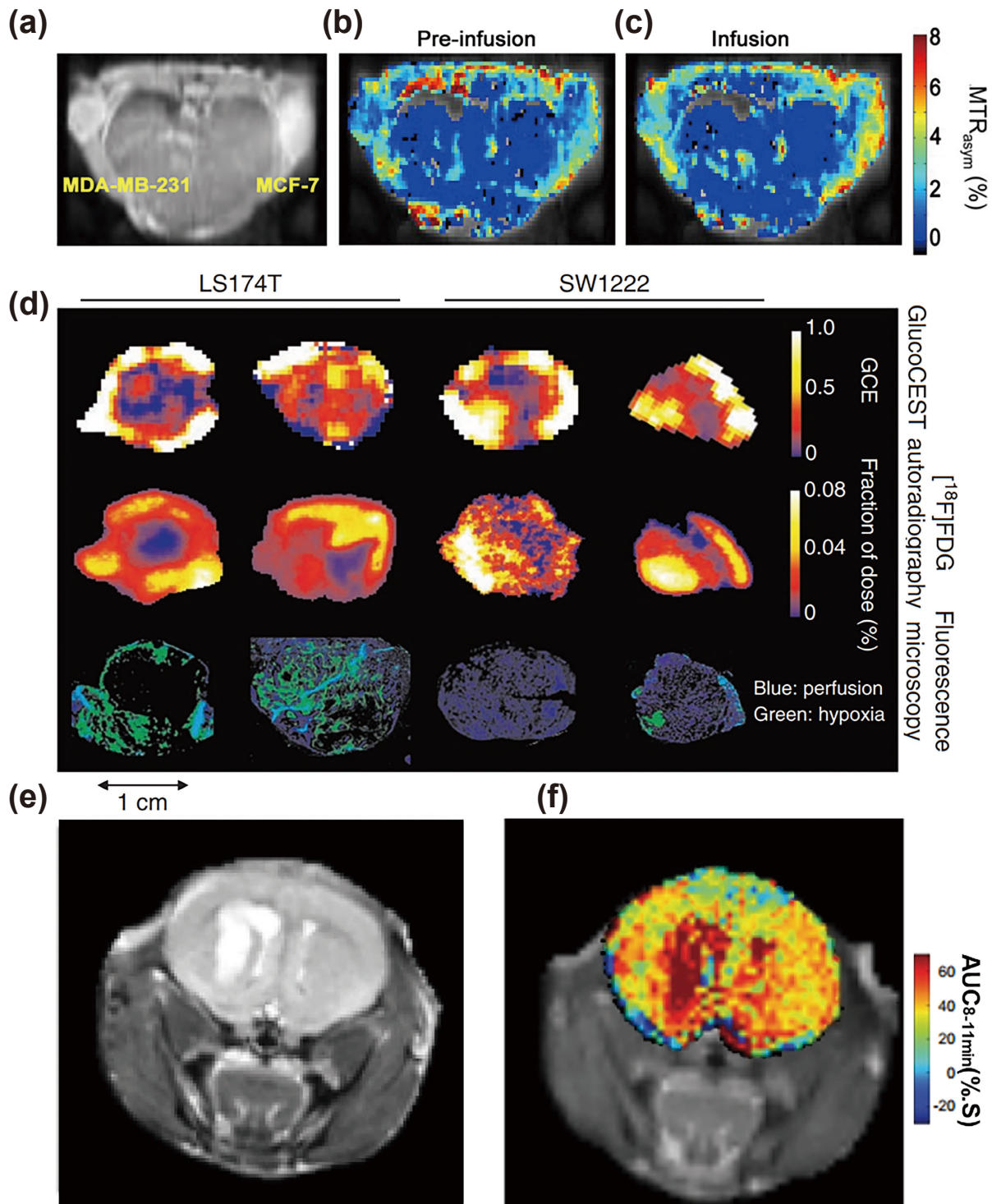
**Fig. 6.** Representative CEST MRI images. (a) The anatomical image of mouse, (b) glucoCEST images before infusing agents, and (c) glucoCEST images after infusing; (d) GlucoCEST images, [¹⁸F]FDG images, and fluorescence images of the same tumor section; (e) the anatomical image and (f) CEST MRI of tumor after injecting 3-OMG for 3–8 min. (a–c) Reprinted with permission from Ref. [17]. Copyright 2012, Wiley Periodicals, Inc. (d) Reprinted with permission from Ref. [28]. Copyright 2013, Springer Nature America, Inc. (e, f) Reprinted with permission from Ref. [32]. Copyright 2019, International Society for Magnetic Resonance in Medicine.

accumulate in the brain and be used to study the metabolism and uptake of sugar (glucose) in brain tumors and neurodegenerative diseases[39]. Xylose is a kind of natural substance that is approved by the United States Food and Drug Administration (FDA) as a sweetener for diabetes. Thus, it has been considered a more biocompatible diaCEST contrast agent than 3-OMG for CEST MRI, especially in brain tissues. In 2020, Wang and his coworkers[40] investigated the CEST

sensitivity of xylose in the rat brain at 9.4 T after xylose administration (Fig. 7a–c) and compared the results of CEST MRI and chemical exchange spin-lock (CESL) MRI. They found that xylose showed better signal intensity, sensitivity, safety and stability in both CEST MRI and CESL MRI when compared with D-glucose[41–43]. They also compared the CEST signal with the CESL signal of xylose and found that the CESL signal was more sensitive than the CEST signal in vivo.

In general, glucose and its analogs have been used in CEST MRI technology for a dozen years and have already been regarded as a new method to study the glucose uptake and metabolic mechanism of cells, for example, monitoring the metabolic changes after neuronal stimulation[44]. Good safety, high resolution and sensitivity, and low cost inspires further improvements of the glucoseCEST sequence, data processing methods, and new glucose-like contrast agents. For example, as an isomer of glucose, mannose can also be used as a diaCEST contrast agent for cell tracking[45]. Since high-mannose (HM) N-glycans are abundant on the surface of human mesenchymal stromal cells (hMSCs) when compared to most other normal and cancer cell lines, mannose-weighted CEST MRI can noninvasively track unlabeled hMSCs after their transplantation (Fig. 7d). This label-free imaging technique for hMSCs may facilitate the development and evaluation of stem cell therapies.

## 4.2 Amide protons

The chemical exchanges between the amino protons in compounds (including proteins, peptides, and polymers) and bulk water protons can generate CEST signals. CEST MRI using amide protons as contrast agents is usually named amide proton transfer (APT) MRI. APT MRI is simpler and safer to image tissues than the other exogenous contrast agents, and the widespread presence of amide protons in the body gives APT MRI sufficient signal intensity for in vivo imaging. Due to the increased mobile protein and peptide content in the tumor regions, APT MRI can distinguish tumor tissues from surrounding normal tissues to detect and diagnose tumor sites[46]. To date, the most common bioapplication of APT MRI technology is the diagnosis of brain tumors, including grading, imaging, and evaluation of the treatment effect for brain cancers.

The APT, or, more accurately, the APT-weighted (APTw) MRI, was first proposed by Zhou et al.[14] in 2003 for imaging brain tumors. As reported, since gliosarcomas (9 L) appear diffuse with unclear regional boundaries in the rat brain, they are hard to distinguish from the surrounding tissues by conventional MRI technologies, such as $T_2$-weighted imaging, $T_1$-weighted imaging, and diffusion-weighted imaging. However, APTw MRI can easily differentiate between tumor tissues and peritumoral tissues to image the tumor region with a distinct boundary. Moreover, the concentration of proteins in tumor tissues can be detected by analyzing the signal intensities of APTw MRI, which can help us to estimate the developmental stage of tumors. They applied the APTw MRI technology to image gliomas in the human brain and demonstrated that APTw can improve tumor detection accuracy and provide more organizational information without using exogenous contrast agents (Fig. 8a)[47]. These endogenous contrast agents (proteins, peptides, etc.) guarantee the safety of patients during the APTw imaging process, accelerating the clinical translation of APTw MRI for tumor patients.
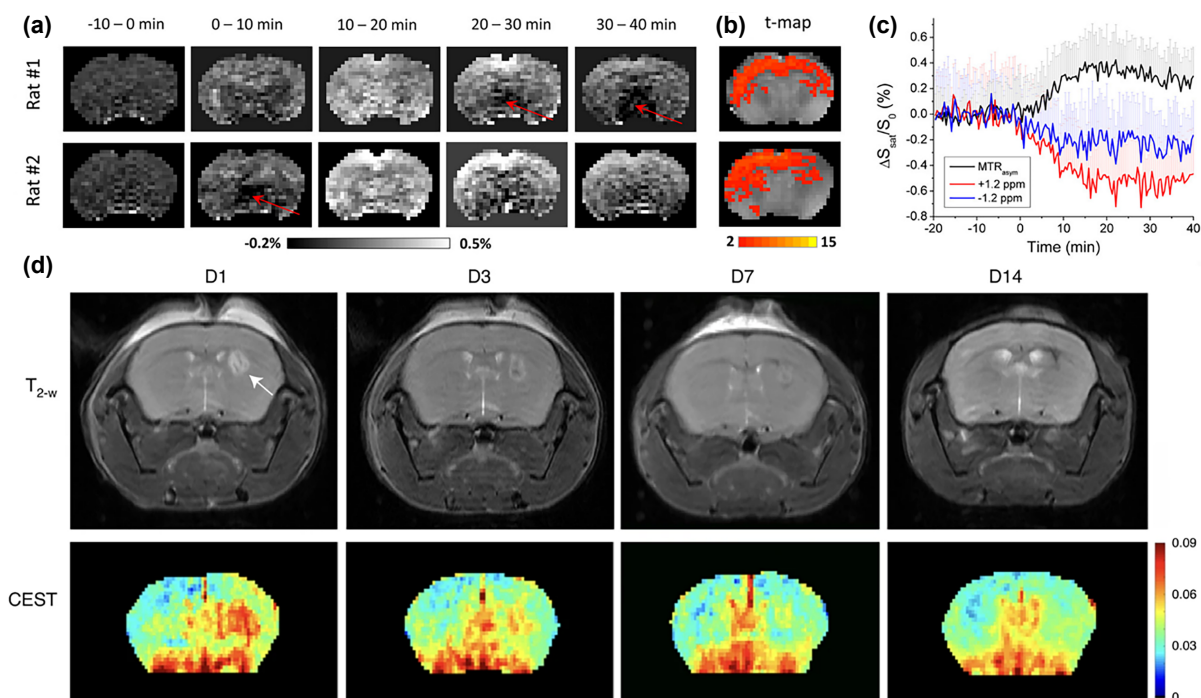


**Fig. 7.** Several images of mouse brains. (a) The glucoCEST imaging, (b) t-map images, and (c) MTR$_{asym}$ analysis of rat brain before and after the injection of xylose. (d) $T_2$-weighted and mannose-weighted CEST MR images of mice after intrastriatal hMSC transplantation. (a–c) Reprinted with permission from Ref. [40]. Copyright 2021, International Society for Magnetic Resonance in Medicine. (d) Reprinted with permission from Ref. [45]. Copyright 2022, The Author(s), under exclusive license to Springer Nature Limited.

In 2014, Yuan et al. employed APTw technology to image tumor tissues in the head and neck regions such as the masseter, parotid, submandibular and thyroid glands and compared the imaging results with the APTw images of normal head and neck tissues[46]. APTw signals were found to be different between tumor tissues and normal tissues from all organs in the head and neck regions. Furthermore, they analyzed the Z-spectrum and APTw images of these tissues to demonstrate the good reproducibility of APTw MRI, which further proves the potential clinical application of APTw technology (Fig. 8b). Compared to brain tumors, head and neck tumor tissues are heterogeneous, and teeth, air-containing structures, and bone will influence the results of APTw imaging. Thus, a spin echo sequence and localized high-order shimming were used to mitigate the field inhomogeneity-induced artifacts to obtain a more accurate signal value and reduce the influence of background noise. A much wider offset frequency sweeping range was required to avoid missing the APTw signal after $B_0$ correction. However, all these sequence changes will prolong the scan time of MRI, so the balance of image quality and acquisition time should be considered in the clinic.

Except for tumor imaging and diagnosis, accurately and efficiently evaluating the therapeutic effect of tumors is also important in clinical research. As we know, concurrent chemotherapy and radiation therapy (CCRT) is an important adjuvant treatment for glioblastoma patients after surgical resection[48]. However, CCRT will cause a treatment-related effect, which is hard to distinguish from tumor progression (TP) by conventional MRI detection methods, even perfusion MRI and diffusion-weighted imaging (DWI). As reported by Park et al.[49], the $APT_w$ MRI displayed a significantly higher signal in the TP than in the treatment-related effect sites, which results from the increase in endogenous mobile proteins and peptides from protein expression in the TP. $APT_w$ MRI is a helpful and facile method to differentiate the TP from the treatment-related effect regions in glioblastoma patients

posttreatment, and the combination of the contrast-enhanced $T_1$ weighted image, perfusion MRI, and APTw imaging can efficiently evaluate the therapy response of glioblastomas (Fig. 9a–c).

Recently, APTw has been widely employed in imaging other diseases such as stroke[50], Alzheimer's disease (AD)[51], Parkinson's disease (PD)[52, 53] and traumatic brain injury (TBI)[54]. Jokivarsi and his coworkers[55] studied APTw imaging of acute cerebral ischemia (ischemic stroke) in 2007. Ischemic stroke is always accompanied by tissue acidosis that exacerbates tissue damage, so that the noninvasive measurement of the pH value in stroke tissues is capable of detecting and grading stroke in vivo. Since the amide proton transfer ratio (APTR) in APTw imaging is influenced by the pH of the surrounding environment, as shown in Fig. 9d and 9e, the APTR will decrease during cerebral ischemia, and there is a correlation between the ΔAPTR (the APTR changes between the ipsilateral and contralateral side) and intracellular pH (pHi) during ischemia. Thus, APTR can delineate acute ischemic stroke areas in the early stage[56], determine tissue viability and damage, and have the potential to help subdivide peri-infarcted tissues. AD is reported to be related to the accumulation of abnormal proteins in the central nervous system[57], such as Tau[58], a-synuclein[59], and TDP-43[60]. Wang et al.[51] first reported the APTw imaging results of AD and compared the APTw signal in the brains of AD patients with that in normal persons; they found that the APTw signal of the hippocampus in AD patients was significantly higher than that in normal persons (Fig. 9f, g). This result showed that the APTw contrast changes in the hippocampus provide information for the diagnosis of AD and even show the severity of AD.

In conclusion, APTw MRI technology is a very useful imaging method that has been widely applied in imaging and diagnosing cancer, stroke, and several neurodegenerative diseases in clinic MRI. However, there are still some challenges that remain in APTw technology, such as the hardware con-
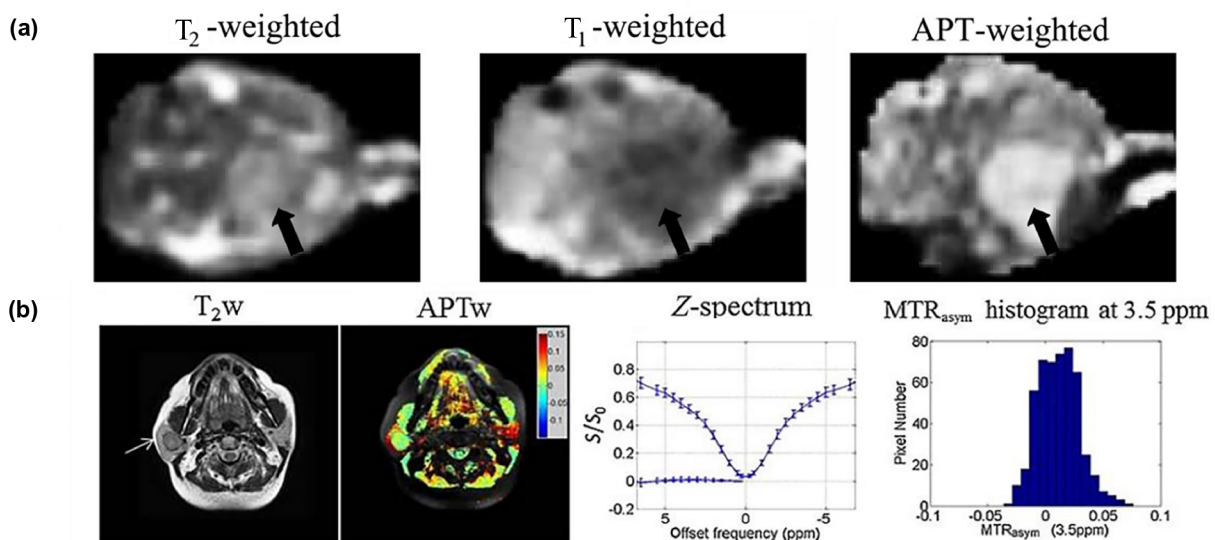


**Fig. 8.** Representative $T_1/T_2$ and CEST MRI images of tumors at different sites. (a) $T_2$-weighted, $T_1$-weighted and APT-weighted images of rat brain tumors; (b) $T_2$-weighted anatomical image and amide proton transfer-weighted image of pleomorphic adenoma in the right parotid gland. (a) Reprinted with permission from Ref. [14]. Copyright 2003, Wiley-Liss, Inc. (b) Reprinted with permission from Ref. [46]. Copyright 2014, John Wiley & Sons, Ltd.

straints of MRI equipment, the complex mechanism of signal generation, and the artifacts from $B_0$ inhomogeneity. Using similar APTw pulse sequences and data processing strategies between hospitals is important to ensure the reproducibility and comparison of diagnosis results[61].

### 4.3 SA and its analogs

To avoid the body tissue background and the signal distraction of water, a larger $\Delta\omega$ between diaCEST agent protons and bulk water protons is preferred to provide better imaging quality and signal intensity. Different from the sugar- and amide-based contrast agents that possess $\Delta\omega$ within approximately 1–3.6 ppm, in 2013, Yang et al[5]. pointed out that the exchangeable protons on SA have a large chemical shift of 9.3 ppm from bulk water protons. The intramolecular hydrogen bonding (IHB) in some salicylic acid analogs can even result in a much larger chemical shift (10.8 ppm) from bulk water protons[62, 63]. From Fig. 10, a large chemical shift (9.3 ppm) was found at the kidney of mice, which is far away from the endogenous metabolites[5]. The signal intensity of the total water is approximately 25% larger at 9.3 ppm than at 5 ppm as a result of less direct saturation. Therefore, SA enhanced the CEST image quality and provided apparent CEST

contrast over the whole kidney. Moreover, it is easy to modify SA with different chemical groups or generate SA nanostructures such as nanoparticles[64] and hydrogels[8] to broaden the application of SA in various drug platforms.

In 2016, on the basis of Yang's research, Lesniak et al.[65] considered the fact that small diaCEST molecules have a high requirement for concentration in practical applications and millimolar levels of contrast agent are required in vivo to produce CEST signals. To solve this problem, they covalently conjugated SA onto the surface of PAMAM dendrimers (Fig. 11a) to build a new kind of diaCEST conjugate with a large $\Delta\omega$ (9.4 ppm) and significantly improved the contrast signal for tumor imaging. They applied this SA-containing dendrimer for CEST imaging of transplanted U87 glioblastoma in rats and showed that the SA polymer was distributed over 50% of the tumor regions with a long retention time of 1.5 h. This method could be used to noninvasively image the accumulation, distribution, and metabolism of nanoparticles in brain tumors with higher spatial resolution and depth penetration to provide a new platform for tracking the process of nano-DDS in tumor treatment. Then, Banerjee et al.[66] developed an amphiphilic smart polymer by grafting SA
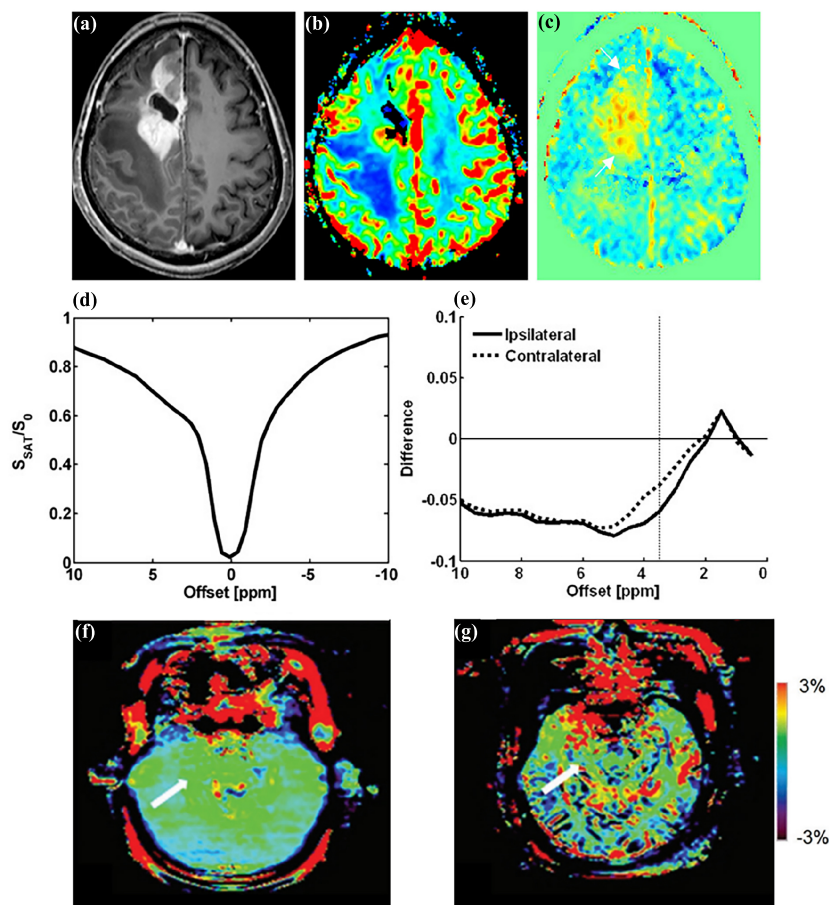


**Fig. 9.** Different MRI images and related analysis. (a) The contrast-enhanced $T_1$-weighted image, (b) dynamic susceptibility contrast (DSC)-enhanced MR image, and (c) APT image of TP. (d) The APTw Z-spectrum and (e) $MTR_{asym}$ result of a stroke patient brain. The APTw image of the brain of (f) a normal person and (g) an AD patient. (a–c) Reprinted with permission from Ref. [49]. Copyright 2016, European Society of Radiology. (d–e) Reprinted with permission from Ref. [55]. Copyright 2007, Wiley-Liss, Inc. (f, g) Reprinted with permission from Ref. [51]. Copyright 2015, Chinese Medical Association.
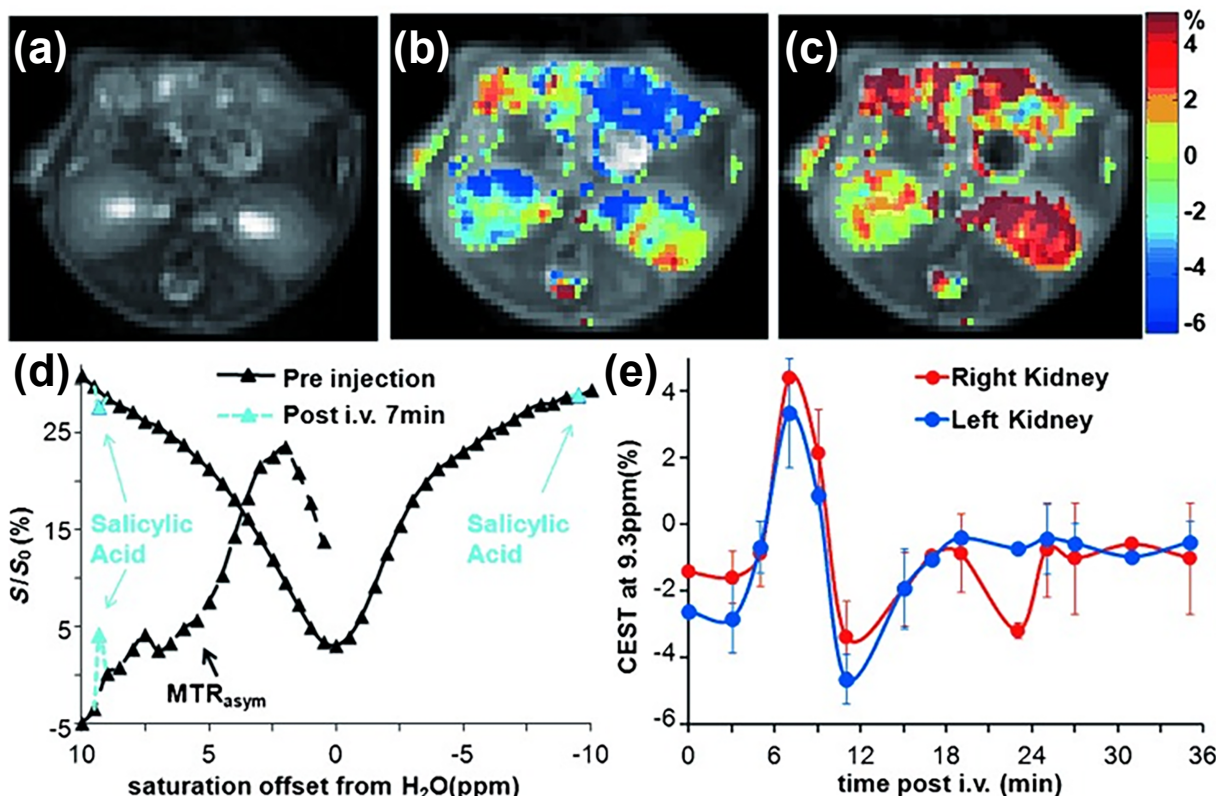
**Fig. 10.** MRI images and related analysis of mice administered SA. (a) $T_2$w image, (b) overlay CEST image preinjection, and (c) overlay CEST image at 7 min postinjection of mice administered SA; (d) Z-spectra and MTR$_{asym}$ for the right kidney before injection (black) and 7 min postinjection (light blue); (e) MTR$_{asym}$ values of the left kidney and right kidney at different time points after SA injection. Reprinted with permission from Ref. [8]. Copyright 2013, Springer Nature Limited.

onto prostate-specific membrane antigen (PSMA)-targeting Lys-urea-Glu conjugated polymaleic anhydride to realize CEST MRI of prostate neoplasia. Fig. 11b shows that this polymeric CEST agent induced a significantly higher CEST signal in PSMA-overexpressing prostate tumor cells than in PSMA-deficient prostate tumor cells, suggesting that it can specifically detect PSMA-overexpressing tumors and provide a new platform for CEST imaging of other biomarkers, such as enzymes and receptors.

Yuan et al.[20] combined Olsa, a salicylic acid analog approved by the FDA for the treatment of inflammatory bowel disease and ulcerative colitis, and the cell penetrating furin substrate peptide RVRR with a click chemistry system to form the "smart" CEST contrast agent Olsa-RVRR (Fig. 11c, d)[67]. Olsa was used in this study as an antitumor drug due to its DNA methylation inhibition effect. Olsa-RVRR can easily penetrate the cell membrane. When it enters HCT116 colon cancer cells with high furin expression, it undergoes furin cleavage and glutathione reduction to expose the 1,2-aminothiol group and initiate click chemistry between the 1,2-aminothiol group and the cyano group of 2-cyanobenzothiazole to form Olsa dimers after the intracellular self-assembly of Olsa dimers to Olsa-NPs by noncovalent π-π stacking interactions[68, 69]. The CEST signal and the antitumor effect of Olsa-RVRR were approximately 6.5- and 5.2-fold higher than those of Olsa for HCT116 tumors, and an excellent "theranostic correlation" was found between the CEST contrast and the therapy effect, which has potential for imaging tumor aggressiveness, drug biodistribution, and therapeutic re-

sponse in the clinic.

The proteases in the tumor extracellular microenvironment play important roles in tumor growth, invasion, migration and angiogenesis[70, 71]. Cathepsin B is a lysosomal cysteine protease of the papain family that is often excreted into the extracellular microenvironment and regarded as a potential biomarker for the early diagnosis of cancers[72]. In 2021, Kombala et al.[73] reported a kind of diaCEST contrast agent with a 5.0 ppm signal from aryl amide protons and a 9.2 ppm signal from SA for evaluating the activity of cathepsin B. When this probe reaches the extracellular microenvironment of the tumor, its aryl amide will be removed by cathepsin B, and the signal at 5.0 ppm will "turn off" (Fig. 11e, f). The signal ratio of SA and aryl amide can hence reflect the activity of cathepsin B in tumor sites and can induce more sensitive signal changes than the diaCEST contrast agent with a single CEST peak.

Due to the large chemical shift from bulk water protons, SA and its analogs have already been a group of important contrast agents for CEST MRI technology. However, the CEST signal of SA is significantly affected by pH, which limits its applications[5]. Due to its easy modification, conjugating SA with some functional groups can not only reduce the influence of pH but also exhibit extra targeting and treatment effects, which will be an important research interest for SA in the future.

## 5 Conclusions and outlook

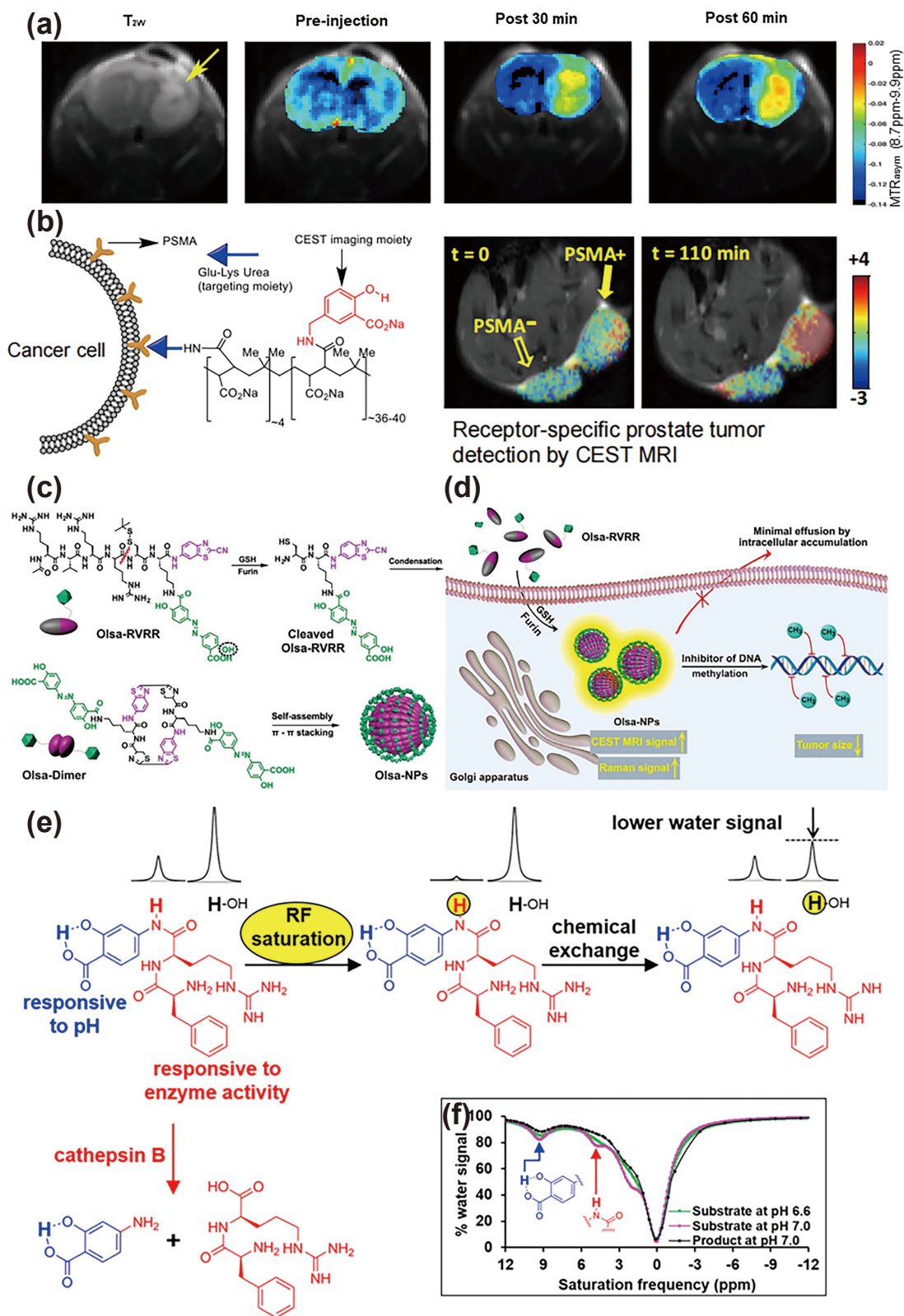In conclusion, CEST MRI is a noninvasive imaging tech-

**Fig. 11.** Several applications of SA, Olsa and other probes. (a) The T$_2$w image and MTR$_{asym}$ image of SA-conjugated dendrimers in vivo: preinjection, 30 min postinjection, and 60 min postinjection; (b) the SA-based polymeric diaCEST agent and its CEST MRI in PSMA(+) PC3 PIP and PSMA(−) PC3 flu tumors; (c) the chemical structure and (d) self-assembly mechanism of Olsa-RVRR in tumor cells. (e) The principle of the cathepsin B-responsive CEST probe; (f) CEST spectra of the cathepsin B-responsive CEST probe before and after cleavage with cathepsin B. (a) Reprinted with permission from Ref. [65]. Copyright 2016, American Chemical Society. (b) Reprinted with permission from Ref. [66]. Copyright 2018, Wiley-VCH Verlag GmbH & Co. KGaA, Weinheim. (c, d) Reprinted with permission from Ref. [22]. Copyright 2019, The Author(s), under exclusive license to Springer Nature Limited. (e, f) Reprinted with permission from Ref. [73]. Copyright 2021, American Chemical Society.

nique with excellent signal sensitivity, frequency selectivity, high spatial resolution, and depth penetration. It has been widely applied in disease imaging, medical diagnosis, nano-DDS, imaging-guided therapy, prognosis examination, etc. Different from $T_1$-weighted, $T_2$-weighted, and paraCEST MRI, which rely on metal ions, or PET and single photon emission computed tomography (SPECT) imaging, which require radioactive tracers, diaCEST imaging utilizes endogenous biomolecules, natural biodegradable agents, FDA-approved drugs, and small organic compounds as CEST contrast contributors, thus possesses some unique advantages in clinical translation, such as low cost, high biocompatibility, and ease of modification.

To enhance the sensitivity and accuracy of diaCEST imaging, various strategies have been developed to minimize the background CEST signals generated by endogenous biomolecules while simultaneously amplifying the signal from diaCEST agents. Therefore, recent studies primarily emphasize the development of diaCEST agents that possess high chemical shifts[5], assembled nanostructures[74], and multimodal imaging capabilities[75]. These advancements also result in a reduction in the required contrast agent dosage and associated biotoxicity concerns. Moreover, imaging of disease biomarkers such as pH[76] and enzymatic activity[77] in vivo has emerged as a key area of research.

Compared with traditional Gd-based contrast agents that have potential risks in the pathogenesis of nephrogenic systemic fibrosis[78] and iron oxide nanoparticle-based contrast agents that may induce immune dysfunction[79], diaCEST agents, particularly natural diaCEST agents (such as glucose, lactate, and amino acids), have low biological toxicity, are easily metabolized, and can be effectively modified, indicating their immense potential for clinical translation. However, there are still many challenges in the further development of diaCEST MRI or CEST MRI technology. Novel diaCEST contrast agents with larger chemical shifts from water are required to reduce the background body CEST signal and direct saturation. Signal enhancement strategies, including in situ self-assembly, polymer conjugation, and CEST detectable hydrogel preperation, are needed to produce sufficient CEST signals at clinical MRI scanners, rather than only at scanners with a high magnetic field. To enlarge the imaging signal and decrease the dosage of contrast agent, diaCEST contrast agent can be conjugated with some targeting motifs to increase the delivery efficiency, such as aptamers, antibodies, receptors, and exosomes. The employment of dual-locked and multimodal contrast agents will improve the specificity and accuracy of CEST imaging. In addition, the gold standard for CEST MRI is needed to unify the MRI scanning sequences and data processing methods between different labs or hospitals to guarantee that the imaging results are reliable and comparable and to boost the application of clinical CEST MRI in more diseases.

## Acknowledgements

## Conflict of interest

The authors declare that they have no conflict of interest.

## Biographies

**Qin Yu** is currently a postgraduate student at the School of Chemistry and Materials Science, University of Science and Technology of China, under the supervision of Prof. Yue Yuan. His research interests include diamagnetism chemical exchange saturated transfer magnetic resonance imaging contrast agents and supramolecular hydrogel.

**Yue Yuan** received her Ph.D. degree in Analytical Chemistry from the University of Science and Technology of China. She is currently a Professor at the University of Science and Technology of China. Her research mainly focuses on diaCEST MRI agents and intracellular self-assembly probes for tumor diagnosis and treatment.

## References

[1] van Zijl P C M, Yadav N N. Chemical exchange saturation transfer (CEST): What is in a name and what isn't? *Magnetic Resonance in Medicine,* **2011**, *65* (4): 927–948.

[2] Heo H Y, Jones C K, Hua J, et al. Whole-brain amide proton transfer (APT) and nuclear overhauser enhancement (NOE) imaging in glioma patients using low-power steady-state pulsed chemical exchange saturation transfer (CEST) imaging at 7T. *Journal of Magnetic Resonance Imaging,* **2016**, *44* (1): 41–50.

[3] Han Z, Liu G. CEST MRI trackable nanoparticle drug delivery systems. *Biomedical Materials,* **2021**, *16* (2): 024103.

[4] Sherry A D, Woods M. Chemical exchange saturation transfer contrast agents for magnetic resonance imaging. *Annual Review of Biomedical Engineering,* **2008**, *10*: 391–411.

[5] Yang X, Song X, Li Y, et al. Salicylic acid and analogues as diaCEST MRI contrast agents with highly shifted exchangeable proton frequencies. *Angewandte Chemie,* **2013**, *125* (31): 8274–8277.

[6] McMahon M T, Bulte J W M. Two decades of dendrimers as versatile MRI agents: A tale with and without metals. *WIREs Nanomedicine and Nanobiotechnology,* **2018**, *10* (3): e1496.

[7] Wang J, Weygand J, Hwang K P, et al. Magnetic resonance imaging of glucose uptake and metabolism in patients with head and neck cancer. *Scientific Reports,* **2016**, *6*: 30618.

[8] Chan K W Y, Liu G, Song X, et al. MRI-detectable pH nanosensors incorporated into hydrogels for in vivo sensing of transplanted-cell viability. *Nature Materials,* **2013**, *12* (3): 268–275.

[9] Delli Castelli D, Terreno E, Aime S. Yb$^{III}$-HPDO3A: A dual pH- and temperature-responsive CEST agent. *Angewandte Chemie International Edition,* **2011**, *50* (8): 1798–1800.

[10] Liu G, Liang Y, Bar-Shir A, et al. Monitoring enzyme activity using a diamagnetic chemical exchange saturation transfer magnetic resonance imaging contrast agent. *Journal of the American Chemical Society,* **2011**, *133* (41): 16326–16329.

[11] Zhang S R, Trokowski R, Sherry A D. A paramagnetic CEST agent for imaging glucose by MRI. *Journal of the American Chemical Society,* **2003**, *125* (50): 15288–15289.

[12] Pavuluri K, McMahon M T. pH imaging using chemical exchange saturation transfer (CEST) MRI. *Israel Journal of Chemistry,* **2017**, *57* (9): 862–879.

[13] Ali M M, Yoo B, Pagel M D. Tracking the relative in vivo pharmacokinetics of nanoparticles with PARACEST MRI.

*Molecular Pharmaceutics,* **2009**, *6* (5): 1409–1416.

[14] Zhou J Y, Lal B, Wilson D A, et al. Amide proton transfer (APT) contrast for imaging of brain tumors. *Magnetic Resonance in Medicine,* **2003**, *50* (6): 1120–1126.

[15] Ferrauto G, Di Gregorio E, Ruzza M, et al. Enzyme-responsive LipoCEST agents: Assessment of MMP-2 activity by measuring the intra-liposomal water 1H NMR shift. *Angewandte Chemie International Edition,* **2017**, *56* (40): 12170–12173.

[16] Davis K A, Nanga R P R, Das S, et al. Glutamate imaging (GluCEST) lateralizes epileptic foci in nonlesional temporal lobe epilepsy. *Science Translational Medicine,* **2015**, *7* (309): 309ra161.

[17] Chan K W Y, McMahon M T, Kato Y, et al. Natural D-glucose as a biodegradable MRI contrast agent for detecting cancer. *Magnetic Resonance in Medicine,* **2012**, *68* (6): 1764–1773.

[18] van Zijl P C M, Jones C K, Ren J, et al. MRI detection of glycogen in vivo by using chemical exchange saturation transfer imaging (glycoCEST). *Proceedings of the National Academy of Sciences of the United States of America,* **2007**, *104* (11): 4359–4364.

[19] Haneder S, Apprich S R, Schmitt B, et al. Assessment of glycosaminoglycan content in intervertebral discs using chemical exchange saturation transfer at 3.0 Tesla: Preliminary results in patients with low-back pain. *European Radiology,* **2013**, *23* (3): 861–868.

[20] Li Y, Chen H, Xu J, et al. CEST theranostics: label-free MR imaging of anticancer drugs. *Oncotarget,* **2016**, *7* (6): 6369–6378.

[21] Liu H, Jablonska A, Li Y, et al. Label-free CEST MRI detection of citicoline-liposome drug delivery in ischemic stroke. *Theranostics,* **2016**, *6* (10): 1588–1600.

[22] Yuan Y, Zhang J, Qi X, et al. Furin-mediated intracellular self-assembly of olsalazine nanoparticles for enhanced magnetic resonance imaging and tumour therapy. *Nature Materials,* **2019**, *18* (12): 1376–1383.

[23] Goffeney N, Bulte J W M, Duyn J, et al. Sensitive NMR detection of cationic-polymer-based gene delivery systems using saturation transfer via proton exchange. *Journal of the American Chemical Society,* **2001**, *123* (35): 8628–8629.

[24] Gilad A A, van Laarhoven H W, McMahon M T, et al. Feasibility of concurrent dual contrast enhancement using CEST contrast agents and superparamagnetic iron oxide particles. *Magnetic Resonance in Medicine,* **2009**, *61* (4): 970–974.

[25] Li J, Feng X, Zhu W, et al. Chemical exchange saturation transfer (CEST) agents: Quantum chemistry and MRI. *Chemistry-A European Journal,* **2016**, *22* (1): 264–271.

[26] Vinogradov E, Keupp J, Dimitrov I E, et al. CEST-MRI for body oncologic imaging: Are we there yet? *NMR in Biomedicine,* **2023**: e4906.

[27] Lin X, Xiao Z, Chen T, et al. Glucose metabolism on tumor plasticity, diagnosis, and treatment. *Frontiers in Oncology,* **2020**, *10*: 317.

[28] Walker-Samuel S, Ramasawmy R, Torrealdea F, et al. In vivo imaging of glucose uptake and metabolism in tumors. *Nature Medicine,* **2013**, *19* (8): 1067–1072.

[29] Rivlin M, Navon G. Glucosamine and N-acetyl glucosamine as new CEST MRI agents for molecular imaging of tumors. *Scientific Reports,* **2016**, *6* (1): 32648.

[30] Nasrallah F A, Pagès G, Kuchel P W, et al. Imaging brain deoxyglucose uptake and metabolism by glucoCEST MRI. *Journal of Cerebral Blood Flow & Metabolism,* **2013**, *33* (8): 1270–1278.

[31] Liu G, Banerjee S R, Yang X, et al. A dextran-based probe for the targeted magnetic resonance imaging of tumours expressing prostate-specific membrane antigen. *Nature Biomedical Engineering,* **2017**, *1* (12): 977–982.

[32] Sehgal A A, Li Y, Lal B, et al. CEST MRI of 3-O-methyl-D-glucose uptake and accumulation in brain tumors. *Magnetic Resonance in Medicine,* **2019**, *81* (3): 1993–2000.

[33] Anemone A, Capozza M, Arena F, et al. In vitro and in vivo comparison of MRI chemical exchange saturation transfer (CEST) properties between native glucose and 3-O-Methyl-D-glucose in a murine tumor model. *NMR in Biomedicine,* **2021**, *34* (12): e4602.

[34] Anemone A, Capozza M, Arena F, et al. In vitro and in vivo comparison of the MRI glucoCEST properties between native glucose and 3OMG in a murine tumor model. bioRxiv: 2021.03. 15.435387, **2021**.

[35] Grasa L, Chueca E, Arechavaleta S, et al. Antitumor effects of lactate transport inhibition on esophageal adenocarcinoma cells. *Journal of Physiology and Biochemistry,* **2023**, *79* (1): 147–161.

[36] Anderson M, Moshnikova A, Engelman D M, et al. Probe for the measurement of cell surface pH in vivo and ex vivo. *Proceedings of the National Academy of Sciences of the United States of America,* **2016**, *113* (29): 8177–8181.

[37] Sweeney M D, Sagare A P, Zlokovic B V. Blood-brain barrier breakdown in Alzheimer disease and other neurodegenerative disorders. *Nature Reviews Neurology,* **2018**, *14* (3): 133–150.

[38] Huntley N F, Patience J F. Xylose: Absorption, fermentation, and post-absorptive metabolism in the pig. *Journal of Animal Science and Biotechnology,* **2018**, *9* (1): 4.

[39] Knutsson L, Xu X, van Zijl P C M, et al. Imaging of sugar-based contrast agents using their hydroxyl proton exchange properties. *NMR in Biomedicine,* **2022**: e4784.

[40] Wang J, Fukuda M, Chung J J, et al. Chemical exchange sensitive MRI of glucose uptake using xylose as a contrast agent. *Magnetic Resonance in Medicine,* **2021**, *85* (4): 1953–1961.

[41] Kim M, Torrealdea F, Adeleke S, et al. Challenges in glucoCEST MR body imaging at 3 Tesla. *Quantitative Imaging in Medicine and Surgery,* **2019**, *9* (10): 1628–1640.

[42] Wu T, Bound M J, Zhao B R, et al. Effects of a D-xylose preload with or without sitagliptin on gastric emptying, glucagon-like peptide-1, and postprandial glycemia in type 2 diabetes. *Diabetes Care,* **2013**, *36* (7): 1913–1918.

[43] Goodwin N C, Mabon R, Harrison B A, et al. Novel L-xylose derivatives as selective sodium-dependent glucose cotransporter 2 (SGLT2) inhibitors for the treatment of type 2 diabetes. *Journal of Medicinal Chemistry,* **2009**, *52* (20): 6201–6204.

[44] Roussel T, Frydman L, Le Bihan D, et al. Brain sugar consumption during neuronal activation detected by CEST functional MRI at ultra-high magnetic fields. *Scientific Reports,* **2019**, *9* (1): 4423.

[45] Yuan Y, Wang C, Kuddannaya S, et al. In vivo tracking of unlabelled mesenchymal stromal cells by mannose-weighted chemical exchange saturation transfer MRI. *Nature Biomedical Engineering,* **2022**, *6* (5): 658–666.

[46] Yuan J, Chen S, King A D, et al. Amide proton transfer-weighted imaging of the head and neck at 3 T: A feasibility study on healthy human subjects and patients with head and neck cancer. *NMR in Biomedicine,* **2014**, *27* (10): 1239–1247.

[47] Zhou J, Blakeley J O, Hua J, et al. Practical data acquisition method for human brain tumor amide proton transfer (APT) imaging. *Magnetic Resonance in Medicine,* **2008**, *60* (4): 842–849.

[48] Fiveash J B, Spencer S A. Role of radiation therapy and radiosurgery in glioblastoma multiforme. *The Cancer Journal,* **2003**, *9* (3): 222–229.

[49] Park K J, Kim H S, Park J E, et al. Added value of amide proton transfer imaging to conventional and perfusion MR imaging for evaluating the treatment response of newly diagnosed glioblastoma. *European Radiology,* **2016**, *26* (12): 4390–4403.

[50] Zhao X, Wen Z, Huang F, et al. Saturation power dependence of amide proton transfer image contrasts in human brain tumors and strokes at 3 T. *Magnetic Resonance in Medicine,* **2011**, *66* (4): 1033–1041.

[51] Wang R, Li S Y, Chen M, et al. Amide proton transfer magnetic resonance imaging of Alzheimer's disease at 3.0 Tesla: A preliminary study. *Chinese Medical Journal,* **2015**, *128* (05): 615–619.

[52] Li C, Peng S, Wang R, et al. Chemical exchange saturation transfer MR imaging of Parkinson's disease at 3 Tesla. *European Radiology,* **2014**, *24*: 2631–2639.

[53] Li C, Wang R, Chen H, et al. Chemical exchange saturation transfer MR imaging is superior to diffusion-tensor imaging in the diagnosis and severity evaluation of Parkinson's disease: A study on substantia nigra and striatum. *Frontiers in Aging Neuroscience,* **2015**, *7*: 198.

[54] Zhang H, Wang W, Jiang S, et al. Amide proton transfer-weighted MRI detection of traumatic brain injury in rats. *Journal of Cerebral Blood Flow & Metabolism,* **2017**, *37* (10): 3422–3432.

[55] Jokivarsi K T, Gröhn H I, Gröhn O H, et al. Proton transfer ratio, lactate, and intracellular pH in acute cerebral ischemia. *Magnetic Resonance in Medicine,* **2007**, *57* (4): 647–653.

[56] Sun P Z, Zhou J, Sun W, et al. Delineating the boundary between the ischemic penumbra and regions of oligaemia using pH-weighted MRI (pHWI). In: Proceedings of ISMRM 14th Scientific Meeting & Exhibition, **2006**.

[57] Xi Q, Zhao X H, Wang P J, et al. Functional MRI study of mild Alzheimer's disease using amplitude of low frequency fluctuation analysis. *Chinese Medical Journal,* **2012**, *125* (5): 858–862.

[58] Kinney J W, Bemiller S M, Murtishaw A S, et al. Inflammation as a central mechanism in Alzheimer's disease. *Alzheimer's & Dementia: Translational Research & Clinical Interventions,* **2018**, *4*: 575–590.

[59] Xu G, Stevens Jr S M, Moore B D, et al. Cytosolic proteins lose solubility as amyloid deposits in a transgenic mouse model of Alzheimer-type amyloidosis. *Human Molecular Genetics,* **2013**, *22* (14): 2765–2774.

[60] Amador-Ortiz C, Lin W L, Ahmed Z, et al. TDP-43 immunoreactivity in hippocampal sclerosis and Alzheimer's disease. *Annals of Neurology,* **2007**, *61* (5): 435–445.

[61] Zhou J, Heo H Y, Knutsson L, et al. APT-weighted MRI: Techniques, current neuro applications, and challenging issues. *Journal of Magnetic Resonance Imaging,* **2019**, *50* (2): 347–364.

[62] Maciel G E, Savitsky G B. Carbon-13 chemical shifts and intramolecular hydrogen bonding. *Journal of Physical Chemistry,* **1964**, *68* (2): 437–438.

[63] Mock W L, Morsch L A. Low barrier hydrogen bonds within salicylate mono-anions. *Tetrahedron,* **2001**, *57* (15): 2957–2964.

[64] Winter P M, Cai K, Chen J, et al. Targeted PARACEST nanoparticle contrast agent for the detection of fibrin. *Magnetic Resonance in Medicine,* **2006**, *56* (6): 1384–1388.

[65] Lesniak W G, Oskolkov N, Song X, et al. Salicylic acid conjugated dendrimers are a tunable, high performance CEST MRI nanoPlatform. *Nano Letters,* **2016**, *16* (4): 2248–2253.

[66] Banerjee S R, Song X, Yang X, et al. Salicylic acid-based polymeric contrast agents for molecular magnetic resonance imaging of prostate cancer. *Chemistry-A European Journal,* **2018**, *24* (28): 7235–7242.

[67] Thomas G. Furin at the cutting edge: From protein traffic to embryogenesis and disease. *Nature Reviews Molecular Cell Biology,* **2002**, *3* (10): 753–766.

[68] Ren H, Xiao F, Zhan K, et al. A biocompatible condensation reaction for the labeling of terminal cysteine residues on proteins. *Angewandte Chemie International Edition,* **2009**, *48* (51): 9658–9662.

[69] Liang G, Ren H, Rao J. A biocompatible condensation reaction for controlled assembly of nanostructures in living cells. *Nature Chemistry,* **2010**, *2* (1): 54–60.

[70] Friedl P, Alexander S. Cancer invasion and the microenvironment: Plasticity and reciprocity. *Cell,* **2011**, *147* (5): 992–1009.

[71] Koblinski J E, Ahram M, Sloane B F. Unraveling the role of proteases in cancer. *Clinica Chimica Acta,* **2000**, *291* (2): 113–135.

[72] Dohchin A, Suzuki J I, Seki H, et al. Immunostained cathepsins B and L correlate with depth of invasion and different metastatic pathways in early stage gastric carcinoma. *Cancer,* **2000**, *89* (3): 482–487.

[73] Kombala C J, Lokugama S D, Kotrotsou A, et al. Simultaneous evaluations of pH and enzyme activity with a CEST MRI contrast agent. *ACS Sensors,* **2021**, *6* (12): 4535–4544.

[74] Lock L L, Li Y, Mao X, et al. One-component supramolecular filament hydrogels as theranostic label-free magnetic resonance imaging agents. *ACS Nano,* **2017**, *11* (1): 797–805.

[75] Law L H, Huang J, Xiao P, et al. Multiple CEST contrast imaging of nose-to-brain drug delivery using iohexol liposomes at 3T MRI. *Journal of Controlled Release,* **2023**, *354*: 208–220.

[76] Qi Q, Fox M S, Lim H, et al. Glucose infusion induced change in intracellular pH and its relationship with tumor glycolysis in a C6 rat model of glioblastoma. *Molecular Imaging and Biology,* **2023**, *25* (2): 271–282.

[77] Sinharay S, Randtke E A, Howison C M, et al. Detection of enzyme activity and inhibition during studies in solution, in vitro and in vivo with catalyCEST MRI. *Molecular Imaging and Biology,* **2018**, *20*: 240–248.

[78] Sieber M A, Lengsfeld P, Walter J, et al. Gadolinium-based contrast agents and their potential role in the pathogenesis of nephrogenic systemic fibrosis: The role of excess ligand. *Journal of Magnetic Resonance Imaging,* **2008**, *27* (5): 955–962.

[79] Geppert M, Himly M. Iron oxide nanoparticles in bioimaging – An immune perspective. *Frontiers in Immunology,* **2021**, *12*: 688927.